Excitation and suppression of chimera states by multiplexing

Vladimir A. Maksimenko,[1] Vladimir V. Makarov,[1] Bidesh K. Bera,[2] Dibakar Ghosh,[2] Syamal Kumar Dana,[3,4] Mikhail V. Goremyko,[1] Nikita S. Frolov,[1,5] Alexey A. Koronovskii,[5] and Alexander E. Hramov[1,5]

[1]*Research and Educational Center "Nonlinear Dynamics of Complex Systems", Yuri Gagarin State Technical University of Saratov, Saratov 410028, Russia*

[2]*Physics and Applied Mathematics Unit, Indian Statistical Institute, Kolkata 700108, India*

[3]*CSIR–Indian Institute of Chemical Biology, Kolkata 700032, India*

[4]*Center for Complex System Research Kolkata, Kolkata, India*

[5]*Faculty of Nonlinear Processes, Saratov State University, Saratov 410012, Russia*

(Received 26 May 2016; revised manuscript received 24 August 2016; published 4 November 2016)

We study excitation and suppression of chimera states in an ensemble of nonlocally coupled oscillators arranged in a framework of multiplex network. We consider the homogeneous network (all identical oscillators) with different parametric cases and interlayer heterogeneity by introducing parameter mismatch between the layers. We show the feasibility to suppress chimera states in the multiplex network via moderate interlayer interaction between a layer exhibiting chimera state and other layers which are in a coherent or incoherent state. On the contrary, for larger interlayer coupling, we observe the emergence of identical chimera states in both layers which we call an *interlayer chimera state*. We map the spatiotemporal behavior in a wide range of parameters, varying interlayer coupling strength and phase lag in two and three multiplexing layers. We also prove the emergence of *interlayer chimera states* in a multiplex network via evaluation of a continuous model. Furthermore, we consider the two-layered network of Hindmarsh-Rose neurons and reveal that in such a system multiplex interaction between layers is capable of exciting not only the synchronous interlayer chimera state but also nonidentical chimera patterns.

DOI: 10.1103/PhysRevE.94.052205

I. INTRODUCTION

Currently, the research on collective behaviors of dynamical systems is focused a great extent on the study of chimera states [1–5] arising in ensembles of identical oscillator models that are abundant in physics and biology. Chimera states, characterized by a coexisting spatial pattern of coherent and incoherent subgroups of dynamical elements in a network, were discovered in 2002 by Kuramoto and Battogtokh [1]. They reported chimera states in a network of nonlocally coupled nonlinear elements described by the complex Ginzburg-Landau system [6] and then demonstrated in a network of the Kuaramoto-Sakaguchi phase model [7]. However, in recent studies, it was shown that such a symmetry breaking of a complete coherent state into chimeralike states can emerge in networks of oscillators with global coupling [5,8,9], and nearest neighbor local coupling [10–12] too. Recent studies further confirm that chimera states are not limited to phase oscillators only, they can emerge in limit cycle and chaotic systems [13], neural systems [14,15], time-discrete map [16], and Boolean networks [17]. As a result, an amplitude-mediated chimera has been proven [3] to be a reality which encourages experimental verification and, in fact, it has now been experimentally evidenced in chemical [18], electronic [19], electrochemical [20], optoelectronic [21], and mechanical [22] systems. However, studies of chimera states were confined so far to the domain of a single-layer network. Among many other effects associated with the emergence of chimera states, important and less studied topics are the stability of chimera states [23], how different isolated networks individually are in any of the states, chimera, coherent, and even incoherent, may be affected when they interact with each other. Obviously, such a situation can appear in real systems, particularly relevant to many areas of science (e.g., neuroscience [24,25]) and technology. Its consideration along with a theoretical investigation demands due attention for prospective practical use [26]. In this paper we address this issue of chimera states in a framework of multilayer networks and explore the resultant effect when they interact with other. Each layer consists of nonlocally coupled identical oscillators and, separately, may be in any of the states, chimera states, coherent, or incoherent states. We consider both the homogeneous network with all identical oscillators and the heterogeneous network where each layer has identical oscillators but heterogeneity of parameters exists between the layers. Such multilayer network structure exists in the real world and has been widely used currently both for the analysis of real data and explaining the multilayer character of real-world networks [27,28]. From the dynamical systems' perspective, the multilayer formulation has been applied to networks whose layers coexist or alternate in time [28]. In both cases, the multilayer formulation allowed synchronization regions that arise as a consequence of the interplay between the layers' topologies and their coupling [29–31], and defined a type of synchronization based on the coordination between the layers [32].

Generally, the multilayer network model is characterized by nodes that have two types of links. One type establishes an intracoupling interaction between the nodes located in the same layer. The second type determines the intercoupling of the dynamic elements between the layers. Depending on the specific objectives of the multilayer configuration, the interlayer relation between the elements of a network may be quite different [29]. We focus on a multilayered network in which interlayer relations match the model described in a recent work [33]. Using this particular multilayer model, we consider a different possible dynamical status: one layer

sustains with chimera states and other layers may be in chimera states, coherent, or incoherent states. We present examples of two-layered and three-layered networks and demonstrate that the original chimera states in isolated networks can be suppressed and recreated by variation of the interlayer coupling strength. Most importantly, we reveal that excitation of the chimera state by multiplexing leads to the emergence of an unknown kind of *interlayer chimera state* where all layers in the network demonstrate the identical chimera pattern. To clarify the presence of the observed phenomena we have studied the continuous model using the Ott-Anttonsen approach, which results showed an excellent match with our numerical simulations. Additionally, we examine the possibility to excite this curious regime in the more realistic network of Hindmarsh-Rose neurons arranged in two multiplexing layers. Indeed, in a certain range of interlayer coupling strengths, this system can exhibit the emergence of a chimera state in a population, which is incoherent without the multiplexing interaction. Moreover, depending on the value of interlayer coupling, a multiplex interaction in this system can excite not only a synchronous (identical through layers) *interlayer chimera state*, but also nonidentical chimera states in interacting layers, that reveals the complexity of emergent phenomena.

II. MULTILAYER NETWORKS

The multilayer network consists of N number of oscillators in each layer where each node in all the layers is represented by the Kuramoto-Sakaguchi (KS) phase model, $\varphi_i^j(t)$ ($i = 1,2,\dots N$; $j = 1,2,\dots M$) is the instantaneous phase of the system; M is the number of layers. Our choice of a dynamical system is motivated by the fact that the nonlocal interaction in a network of KS phase oscillators is a paradigm of chimera states [1,7] and since we focus here on chimera states in the multilayered networks. A schematic diagram of a two-layered network is shown in Fig. 1(a) where each node in each layer has two types of links: (1) intralayer links (solid lines), and (2) interlayer links (dashed lines). The intralayer links establish a nonlocal interaction within the elements of the same layer and the interlayer links connect the elements between the layers. The phase dynamics of each node φ_i^j (ith node, jth layer) in the multilayer network is described by

$$\frac{d\varphi_i^j}{dt} = \omega_i^j - \frac{\lambda_1^j}{2P^j+1}\sum_{k=i-P^j}^{i+P^j}\sin\left(\varphi_i^j - \varphi_k^j + \alpha^j\right) + \frac{\lambda_2}{M}\sum_{l\neq j}\sin\left(\varphi_i^j - \varphi_i^l\right), \quad (1)$$

where ω_i^j is the natural frequency of the ith oscillator in the jth layer, λ_1^j and λ_2 define the intra- and interlayer coupling strengths respectively, $R^j = P^j/N$ is defined as the coupling radius where P^j is the number of neighboring oscillators each oscillator is connected to, in both directions, in a jth layer; α^j is a phase lag parameter identical for all the oscillators in the jth layer but can be chosen different in different layers to create heterogeneity. We consider $\omega_i^j = 1.0$ for all the oscillators of all the layers. In the absence of interlayer coupling, i.e., $\lambda_2 = 0$, individual networks of phase oscillators (1) demonstrate chimera states when the value of α^j remains close to $\pi/2$ (more precisely, for $\alpha^j \in [1.45; 1.57]$) for an appropriate choice of λ_1^j.

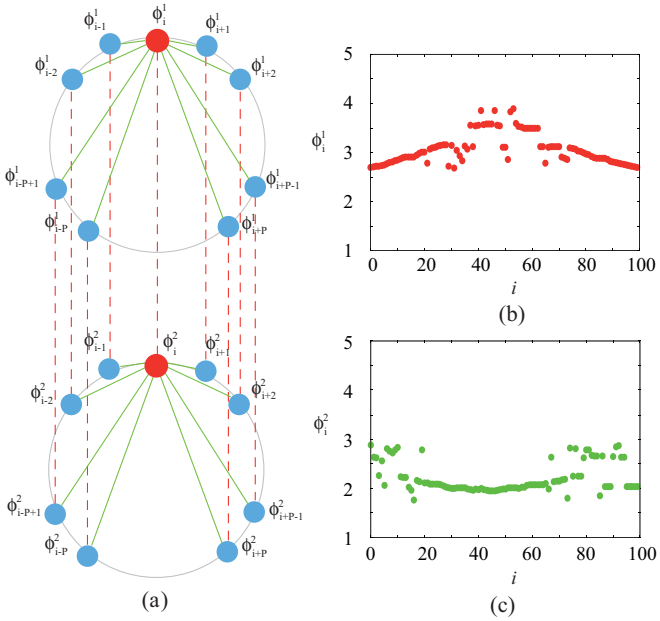

FIG. 1. (a) Schematic diagram of inter- (dashed lines) and intralayer (solid lines) links in a two-layered network whose node dynamics is governed by phase oscillators and snapshots of phase distributions φ_i^j for all the oscillators (i), illustrating the occurrence of chimera states in the first (b) and the second (c) layers in absence of interlayer coupling links. For illustration of nonlocal coupling, we mark one node in each layer by a red circle which is connected to its nearby neighbors on both sides within a radius $R^1 = R^2 = R$, where $R = 0.35$. Each node is actually connected to nearby nodes by similar manner at equal radius but not shown here for clarity of picture. Each node in the upper layer is connected to its immediate bottom node in lower layer.

For simplicity, we first consider the multiplex network as consisting of two layers, $M = 2$. For this two-layered network, we take the intralayer coupling strength as $\lambda_1^1 = \lambda_1^2 = \lambda_1$. By a choice of $\alpha^1 = \alpha^2 = 1.45$ and $\lambda_2 = 0$, one can easily obtain chimera states on both the layers as shown earlier [1,2]. Snapshots of phase distribution in the two layers are shown separately in Figs. 1(b) and 1(c) respectively for $P = 35$, $\lambda_1 = 0.085$. Two different spatial chimera patterns emerge in two isolated layers due to a different choice of initial distributions of phases in the layers,

$$\varphi_i^1(0) = \begin{cases} \pi\left(\frac{4i}{N} - 1\right), & i \in \left[0, \frac{N}{2}\right] \\ \pi\left(3 - \frac{4i}{N}\right), & i \in \left[\frac{N}{2} + 1, N\right] \end{cases}, \quad (2)$$

$$\varphi_i^2(0) = \begin{cases} \pi\left(1 - \frac{4i}{N}\right), & i \in \left[0, \frac{N}{2}\right] \\ \pi\left(\frac{4i}{N} - 3\right), & i \in \left[\frac{N}{2} + 1, N\right]. \end{cases} \quad (3)$$

We added small random fluctuations in the initial conditions in both the layers. In order to confirm the existence of chimera states, we use a statistical measure, a strength of incoherence SI^j [34] from a local standard deviation analysis, separately

for both the layers. The SI^j is defined as

$$\mathrm{SI}^j = \frac{\sum_{r=1}^{m} \Theta\left(\delta^j - \sigma_r^j\right)}{m}, \tag{4}$$

where $\Theta(\bullet)$ is the Heaviside step function, δ^j is a predefined threshold value, m is the number of oscillators in each group of equal length $n = N/m$, for which the local standard derivation σ_r^j is calculated as

$$\sigma_r^j = \left\langle \sqrt{\frac{1}{n} \sum_{s=n(r-1)+1}^{rn} \left(\varphi_i^j - \Phi^j\right)^2} \right\rangle_t. \tag{5}$$

Here $\langle \bullet \rangle_t$ denotes averaging over time and Φ^j corresponds to the phase averaged over all the oscillators in jth layer. A value of $\mathrm{SI}^j = 0$ in each layer represents a coherent state while $\mathrm{SI}^j = 1$ and $0 < \mathrm{SI}^j < 1$ represents incoherent and chimera states respectively.

III. EFFECT OF MULTIPLEXING: PHASE OSCILLATORS

To demonstrate the interaction between the layers with different chimera patterns shown in Fig. 2(b) (keeping $\lambda_1^{1,2} = 0.085$, $P = 35$), we increase the interlayer coupling strength λ_2 and observe the changes in the spatial pattern in both the layers. The dependencies of $SI^{1,2}$ on the interlayer coupling strength λ_2 are presented in Fig. 2(a) (upper panel) in cross (+) and solid lines.

One can see that an increase of interlayer interaction leads to fluctuations, which, obviously, corresponds to the variation of the number of elements, involved in the coherent and

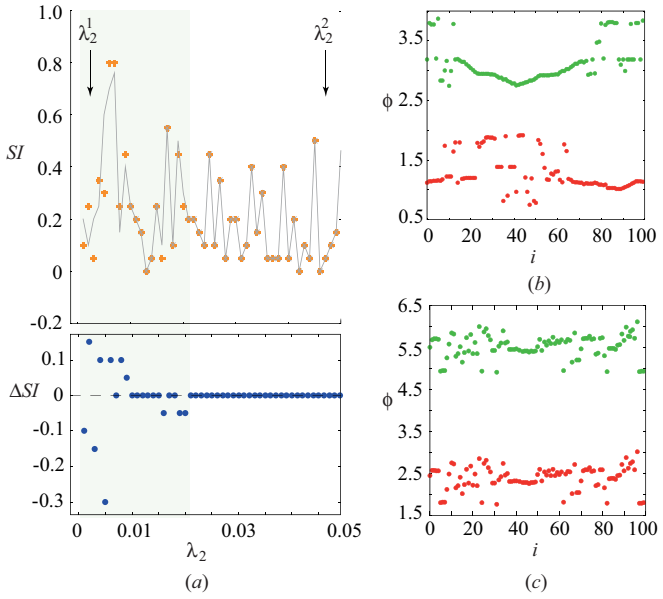

FIG. 2. (a) Strength of incoherence SI of upper layer (+) and lower layer (solid line) in Fig. 1 against the interlayer coupling strength λ_2, a difference $\Delta\mathrm{SI} = \mathrm{SI}_1 - \mathrm{SI}_2$ between the layers obtained for the same range of λ_2. Snapshots of phase distributions obtained for (b) asynchronous chimera states, $\lambda_2 = \lambda_2^1 = 0.001$, (c) synchronous chimera states, $\lambda_2 = \lambda_2^2 = 0.045$. Locations of control points, λ_2^1,λ_2^2 are shown by the arrows. $\alpha^{1,2} = 1.45$.

incoherent subclusters. At the same time, both the values of SI^1 and SI^2 remain confined to the interval $(0,1)$, which evidence that chimera states exist in both the layers for a wide range of λ_2. In order to identify the relation between the chimera states in different layers, we calculate the difference between the strength of incoherence in each layer as $\Delta\mathrm{SI} = \mathrm{SI}^1 - \mathrm{SI}^2$. For low values of λ_2, ΔSI fluctuates indicating incoherence between the two layers although individually they show chimera states as clear from Fig. 2(b). For increasing λ_2, ΔSI becomes zero intermittently and is finally stabilized at zero for $\lambda_2 > 0.02$ as shown in Fig. 2(a) and this state is characterized by the emergence of synchronous chimera states which we define as interlayer chimera states. One can see that an increase of interlayer coupling makes a transformation of chimera states on both the layers [cf. initial states in Figs. 1(b) and 1(c)] from an asynchronous to synchronous chimera states. The phase distributions corresponding to the cases of spatially asynchronous and synchronous dynamics of the layers are shown in snapshots in Figs. 2(b) and 2(c) respectively. We can easily locate coherent and incoherent subpopulations from the snapshots (upper and lower plots) of instantaneous phases of two oscillator populations ($N = 100$) in Fig. 2(b) where their locations are different leading to asynchronous chimera patterns. However, the chimera patterns are exactly the same in Fig. 2(c) for a larger $\lambda_2 = 0.045$.

Next we consider a heterogeneous system of two layers when one layer survives with the chimera state as defined above while the other one is changed to be either in a coherent or an incoherent state in isolation ($\lambda_2 = 0$). We address the question once again of what happens when they start multiplexing. In order to obtain coherent or incoherent states in the ensemble of phase oscillators (1), we tune the phase lag parameter α^2 of the oscillators in the lower layer while $\alpha^1 = 1.45$ is kept unchanged in the upper layer to maintain chimera states. It is known that, for our choice of $\lambda_1^{1,2} = 0.085$, chimera states emerge in a range of $\alpha^j \in [1.45; 1.57]$ while for $\alpha^j < 1.45$ and $\alpha^j > 1.57$, the oscillators demonstrate coherent and incoherent behavior respectively. Accordingly, we consider two cases, the lower layer in the multilayer network (1) is in (I) a coherent state for $\alpha^2 = 1.2$, (II) an incoherent state for $\alpha^2 = 1.7$.

The phase distribution of all oscillators in both layers is shown in Fig. 3 for two different cases (case I: upper row, $\alpha^1 = 1.45$, $\alpha^2 = 1.2$; case II: bottom row, $\alpha^1 = 1.45$, $\alpha^2 = 1.7$). Snapshots of instantaneous phases of all the oscillators, in both upper and lower panels, are plotted for different values of interlayer coupling: (a) $\lambda_2 = 0$, (b) $\lambda_2 = 0.2$, (c) $\lambda_2 = 0.5$. For case I, we find, in the upper panels, suppression and re-emergence of chimera states with increasing λ_2. In the absence of interlayer coupling $\lambda_2 = 0$, the upper layer shows chimera states (red dots) and the lower layer exhibits a coherent state (green dots) as shown in the left panel. With increasing λ_2, the chimera state in the upper layer is destabilized and, most interestingly, passes through a phase of intralayer as well as interlayer coherence for an intermediate $\lambda = 0.2$ [upper panel in Fig. 3(b)] with complete suppression of chimera states. However, for a larger $\lambda_2 = 0.5$ the chimera pattern re-emerges in both layers when an interlayer synchrony is established [upper panel in Fig. 3(c)]. Additionally, we explore case II when the upper layer is still kept in chimera states, however,

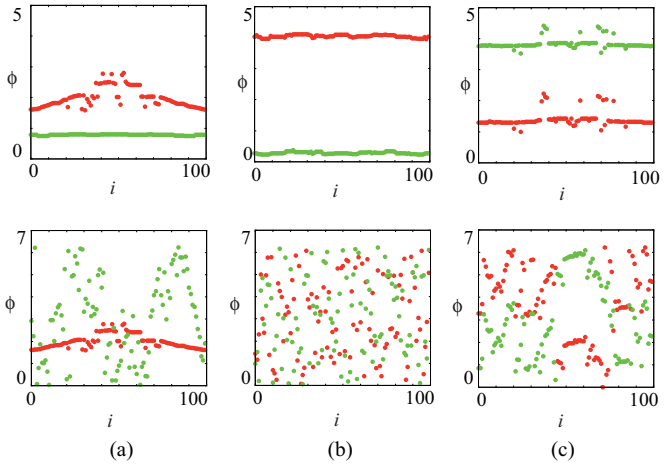

FIG. 3. Multiplexing of layers: chimera-coherent layers (upper row, $\alpha^1 = 1.45, \alpha^2 = 1.2$) and chimera-incoherent layers (lower row, $\alpha^1 = 1.45$, $\alpha^2 = 1.7$). Snapshots of instantaneous phases of all the oscillators (in both layers) are presented in the upper and lower panels for different values of λ_2: (a) $\lambda_2 = 0$, (b) $\lambda_2 = 0.2$, (c) $\lambda_2 = 0.5$.

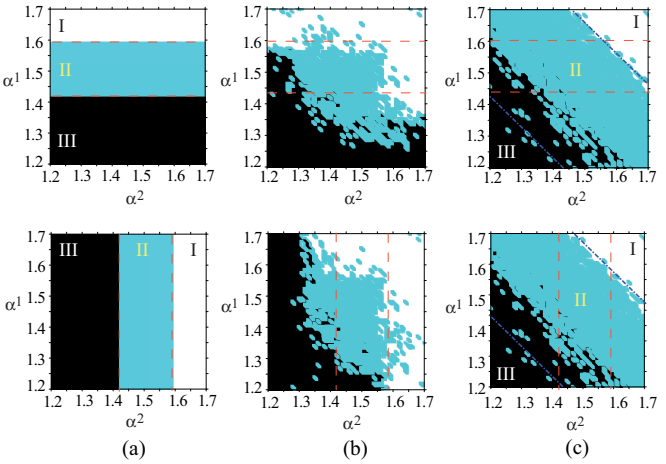

FIG. 4. Phase diagram in the phase lag parameter plane (α^1,α^2) where strength of incoherent is used for the first layer, SI^1 (upper row) and the second layer, SI^2 (bottom row) to measure different patterns. Plots in any row (upper or lower panels) are obtained for the different values of interlayer coupling strength, (a) $\lambda_2 = 0.0$, (b) $\lambda_2 = 0.02$, (c) $\lambda_2 = 0.5$. The areas, corresponding to the incoherent, chimera, and coherent state are marked as I (white), II (blue), and III (black) respectively.

the lower layer is pushed to the incoherent state by a choice of $\alpha^2 = 1.7$, in the absence of interlayer coupling [lower panel in Fig. 3(a)]. With an increase of λ_2, as shown in the series of lower panels, the chimera states in the upper layer are again suppressed for an intermediate λ_2 value. But, in contrast to complete coherence in both the layers as seen in case I, the double layered network develops both intralayer and interlayer incoherence for an intermediate $\lambda_2 = 0.2$ value [lower panel in Fig. 3(b)], however, the synchronous interlayer chimera states emerge for larger $\lambda_2 = 0.5$ [lower panel in Fig. 3(c)]. It should be noted that the obtained results remain valid for the multilayer network of nonidentical oscillators where the degree of heterogeneity is low enough to keep chimera states initially stable on both layers.

We determine the $SI^{1,2}$ values for both the layers in the parameter plane (α^1, α^2) and plot them in phase diagrams for different values of λ_2 in Fig. 4. The regions corresponding to the incoherent, the chimera and the coherent states are marked as I (white region), II (gray region) and III (black region) respectively for $\lambda_2 = 0$. Figure 4(a) shows that, in the absence of interlayer interaction, the chimera states can be obtained in both layers for ranges of values, $\alpha^1 \in [1.45; 1.57]$ and $\alpha^2 \in [1.45; 1.57]$ respectively. Clear boundaries exist in the phase diagrams delineating the incoherent, coherent, and chimera state (the area between two red dashed lines) regimes. With the increase of coupling strength λ_2, the layers start to interact leading to the transformation of the phase diagrams in the (α^1,α^2) plane as shown in Fig. 4(b). The boundaries become of a fractal nature in both upper and lower panels in Fig. 4(b), however, we still find a broad parameter regime of chimera states. Finally, when the coupling strength is large enough, the boundaries become much smoother once again as shown in Fig. 4(c) where both layers demonstrate chimera states for some relations between α^1 and α^2 where synchronous chimera states emerge. For comparison, the parameter regions of chimera states in isolated layers are still marked by horizontal red dashed parallel lines in Figs. 4(b) and 4(c). The interacting layers demonstrate chimera states for those $\alpha^{1,2}$ values, which otherwise correspond to the coherent or the incoherent dynamics in the absence of interlayer links or vice versa exhibit fully coherent or incoherent states for $\alpha^{1,2} \in [1.45; 1.57]$.

Finally, we extend our results to a three-layered multiplexing network ($M = 3$) as shown in Fig. 5. The initial phases of the oscillators in the third layers are arranged accordingly,

$$\varphi_i^3(0) = \begin{cases} \pi - \frac{8\pi i}{N}, & i \in \left[0, \frac{N}{4}\right], \\ -\pi + 2\pi\left(\frac{4i-N}{N}\right), & i \in \left[\frac{N}{4}+1, \frac{N}{2}\right], \\ \pi - 4\pi\left(\frac{2i-N}{N}\right), & i \in \left[\frac{N}{2}+1, \frac{3N}{4}\right], \\ -\pi + 2\pi\left(\frac{4i-3N}{N}\right), & i \in \left[\frac{3N}{4}+1, N\right] \end{cases} \quad (6)$$

with additive small random fluctuations.

The strength of incoherence SI^{1-3} in the parameter plane (α^3,α^*) is shown in Fig. 6 for all three layers in absence of the interlayer coupling (left column) and for strong inter-layer interaction ($\lambda_2 = 0.5$) (right column). The surfaces within the columns correspond to the first (a), second (b), and third (c) layers respectively. The value of $\alpha^* = \alpha^{1,2}$ corresponds to the simultaneous change of the α parameter in the first and second layers. All three layers are synchronized for large interlayer coupling strength and demonstrate a synchronous interlayer chimera state for the same values of the phase lag. The addition of a third layer leads to a broadening of the parameter space of interlayer chimera states. Moreover, similar behavior is observed in further increasing of the number of layers in this multiplex network.

IV. ANALYTICAL RESULTS

We carry out an analytical study of the multiplex network of phase oscillators and show that the observed chimera patterns do not depend on the number of oscillators in each layer. We restrict our analysis to a multilayer network of

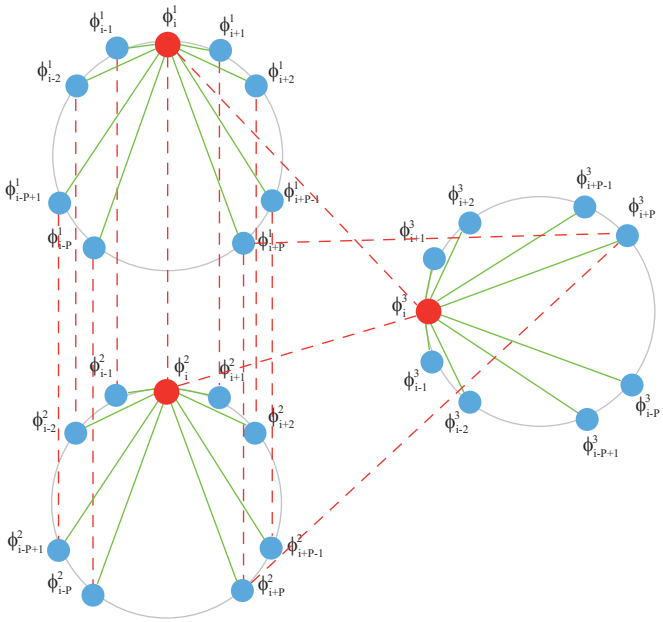

FIG. 5. A schematic diagram of multiplex network with three layers. Each layer is nonlocally connected with $P^{1,2,3} = P$ number of neighbors in each direction. The interlayer connections between the layers 1 and 3 are shown by dashed lines. Note that only few nodes from second to first layer and third to first layer are only shown for clarity of picture. In reality, all nodes in each layer are connected to its immediate bottom node.

two interacting layers. We have applied the Ott-Antonsen (OA) approach [35–38] to reduce the infinite-dimensional network of the Kuaramoto-Sakaguchi phase model to the systems of two-dimensional differential equations. Although OA anzatz is generally used in the case of coupled nonidentical oscillators with different natural frequencies, this method is also effectively applied to the analysis of homogeneous networks [39–42].

In the framework of this approach we describe the dynamics of the network in terms of probability density function (PDF), defined for both the layers of the multiplex network as $f^1(x,\varphi,t)$ and $f^2(x,\varphi,t)$. As the number of oscillators is constant in time we can write the continuity equation for PDF,

$$\frac{\partial f^{1,2}}{\partial t} + \frac{\partial (f^{1,2} v^{1,2})}{\partial \varphi^{1,2}} = 0, \tag{7}$$

where $v^{1,2}$ according to (1) is

$$v^{1,2} = \frac{d\varphi^{1,2}}{dt} = \omega - \frac{1}{2t}\{r^{1,2} e^{\imath\varphi^{1,2}} - \bar{r}^{1,2} e^{-\imath\varphi^{1,2}}\}; \tag{8}$$

the overbar indicates complex conjugate and r is the order parameter written in the following form:

$$r^{1,2} = e^{\imath\alpha_{1,2}} \frac{\lambda_1}{2R} \int_0^1 G(x-y) \int_0^{2\pi} f^1(y,\varphi,t) e^{-\imath\varphi} d\varphi dy - \frac{\lambda_2}{2} \int_0^1 \delta(x-y) \int_0^{2\pi} f^2(y,\varphi,t) e^{-\imath\varphi} d\varphi dy, \tag{9}$$

where $G(x-y)$ is the intralayer coupling kernel,

$$G(x-y) = H\{\cos[(x-y)2\pi] - \cos(R^{1,2}2\pi)\}. \tag{10}$$

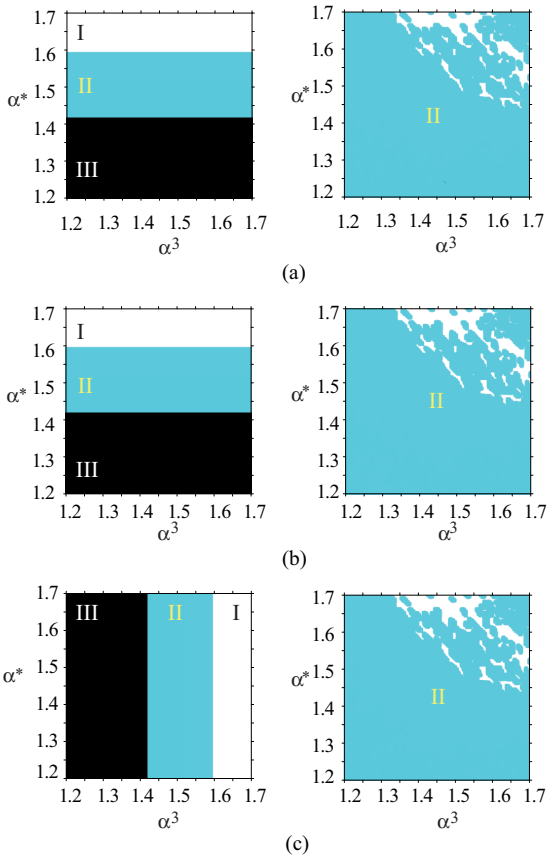

FIG. 6. The strength of incoherent, calculated for the (a) first SI^1, (b) second SI^2, and (c) third SI^3 layers for different values of the phase lag parameters (α^*,α^3), where $\alpha^* = \alpha^{1,2}$. The plots within a column are obtained for the different values of interlayer coupling strength λ_2: $\lambda_2 = 0.0$ (left column) and $\lambda_2 = 0.5$ (right column)

The coupling kernel $G(x-y)$ written in this form perfectly fits the way of intralayer nonlocal coupling in our numerical simulation. $H(x)$ in (10) is the Heaviside step function. We are looking for the solution $f^{1,2}(x,\varphi,t)$ in the form of Fourier series taking into account the OA ansatz $f_n(x,\varphi,t) = a(x,\varphi,t)^n$:

$$f^{1,2}(x,\varphi,t) = \frac{1}{2\pi}\left(1 + \sum_{n=1}^{\infty}\{a(x,t)^{1,2}\}^n e^{\imath n\varphi} + \text{c.c.}\right). \tag{11}$$

Substituting (8)–(11) to (7) we obtain the final equation,

$$\frac{\partial a^{1,2}}{\partial t} + \imath\omega a^{1,2} + \frac{1}{2}[\bar{r}\{a^{1,2}\}^2 - r] = 0, \tag{12}$$

where the order parameter with respect to the OA ansatz becomes

$$r^{1,2}(x,t) = \frac{\lambda_1}{2R} \int_0^1 G(x-y) a^{1,2}(y,t) dy - \frac{\lambda_2}{2} \int_0^1 \delta(x-y) a^{2,1}(y,\varphi,t) dy. \tag{13}$$

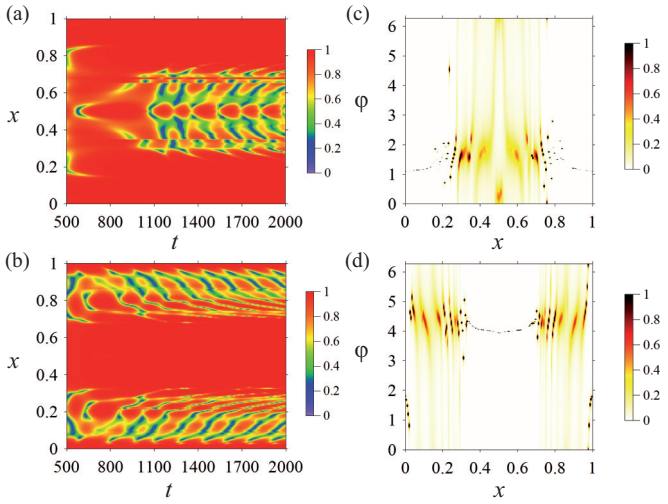

FIG. 7. Spatiotemporal evolution of $|a|^1$ (a) and $|a|^2$ (b) in two layers. Phase distributions $f^1(x,\varphi)$ (c) and $f^2(x,\varphi)$ (d) after finishing the transient process. Plots are obtained for $\alpha^{1,2} = 1.45$, $R^{1,2} = 0.35$, $\lambda_1 = 0.085$, $\lambda_2 = 0$.

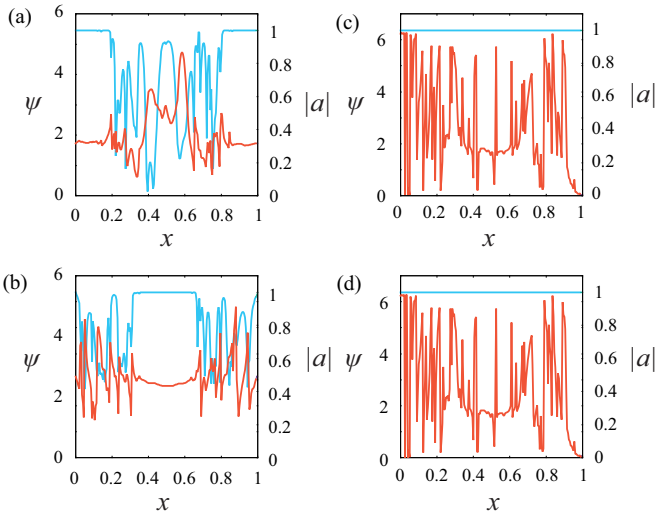

FIG. 8. Snapshots of the upper layer (upper row) and the lower layer (bottom row) states at the different vales of interlayer coupling: (a),(b) $\lambda_2 = 0.015$, (c),(d) $\lambda_2 = 0.045$.

To determine the phase distribution we substitute OA ansatz $a^{1,2} = |a|^{1,2}e^{-j\psi^{1,2}}$ to (11):

$$f^{1,2}(x,\varphi,t) = \frac{1}{2\pi}\frac{1-\{|a|^{1,2}\}^2}{(1-|a|^{1,2})^2+2|a|^{1,2}\big(1-\cos[\varphi-\psi^{1,2}]\big)}. \quad (14)$$

Here $|a|^{1,2}$ is a maximum value of the phase distribution and $\psi^{1,2}$ is a phase value corresponding to the distribution maximum.

Let us discuss the results that we have obtained in the framework of the analytical model. In Figs. 7(a) and 7(b) we present the space-time evolution of $|a|^{1,2}$ for the different layers in the absence of coupling between two layers. The spatial distributions of phase $f^{1,2}(x,\varphi)$ are also presented in Figs. 7(c) and 7(d). One can easily compare these plots with the results of the numerical simulation shown in Fig. 1. With the same network parameters $\alpha^{1,2} = 1.45$, $R^{1,2} = 0.35$, $\lambda_1 = 0.085$, $\lambda_2 = 0.0$ and initial conditions we observe the same behavior on different layers of the multiplex network. After the transient process, the chimera patterns emerge in both layers. Wherein the first layer is characterized by the coherent phase regions at two ends and the incoherent pattern in the middle, at the same time, the inverse chimera pattern sets in the second layer. It is clear that the analytical model based on the assumption of an infinite number of oscillators perfectly describes the network behavior and repeats the results of numerical simulation of $N = 100$ Kuramoto-Sakaguchi phase oscillators. At the same time, we have numerically analyzed the network of $N = 2000$ KS oscillators and obtained the same results of coherent pattern formation.

The introduction of interlayer coupling to the analytical model gives us the following results. In Fig. 8 the snapshots of the layers at different values of interlayer coupling level are presented. In this case, it is more suitable to analyze the behavior of the complex OA ansatz $a^{1,2}(x)$ in terms of its absolute value $|a|^{1,2}(x)$ and argument $\psi^{1,2}(x)$ distributed in space. At low values of interlayer coupling strength $\lambda_2 = 0.015$, we observe the asynchronous interlayer chimera between the upper [Fig. 8(a)] and lower layers [Fig. 8(b)]. In this case the chimera state does sufficiently differ from one obtained in the absence of interlayer coupling. It is still characterized by the existence of coherent and incoherent areas herewith with $|a| < 1$ and the randomly distributed phase ψ in the incoherent region. Increasing the value of interlayer coupling strength $\lambda_2 = 0.045$ leads to the synchronous chimera state between the upper and lower layers and both of them demonstrate identical behavior [Figs. 8(c) and 8(d)]. It is easy to see that in general the phase is randomly distributed over the space but nevertheless the small areas of coherent dynamics exist: we obtain the *interlayer chimera state*. Notably, in spite of the random phase distribution the absolute value $|a|$ equals 1 all over the space. It means that the synchronization between layers totally determines the phase behavior at any point of space and the phase distribution $f^{1,2}(x,\varphi)$ has a form close to Dirac δ function centered at phase $\psi(x)$ as $|a|(x) \to 1$. It becomes clear that from the point of view of intralayer interaction this state is incoherent but the coherence appears between interacting layers. Such behavior of a multiplex Kuramoto-Sakaguchi phase oscillator network with nonlocal coupling described by means of an analytical model coincides with the results obtained in the framework of numerical simulation (Fig. 2). So the analytical study of the interlayer network interaction confirms the existence of the synchronous *interlayer chimera state* behavior observed during the numerical simulation.

V. MULITLAYER NETWORK: HINDMARSH-ROSE NEURONAL MODEL

We also reveal the observed phenomena in a more realistic two-layered multiplex network of the Hindmarsh-Rose (HR) neuron systems. This HR model is more realistic because depending upon the parameter values, an individual oscillator exhibits different types of behaviors, such as square-wave

bursting (chaotic and periodic), mixed mode bursting, spiking, and plateau bursting, etc. Recently, existence of chimera states was reported in a single layer network of HR-neuronal models using nonlocal [10,14] and local [43] coupling interaction. Here we show how multiplex interaction between layers of Hindmarsh-Rose neurons influences chimera states in the system, and examine the effect of delay in this coupling.

We consider a network consisting of two multiplexing layers of 100 HR systems with more realistic chemical synaptic nonlocal intralayer interaction and interlayer synaptic coupling with the presence of delay τ,

$$\begin{aligned}
\dot{x}_i^j &= a\left(x_i^j\right)^2 - \left(x_i^j\right)^3 - y_i^j - z_i^j \\
&\quad + \frac{\lambda_1^j}{2P^j}\left(v_s - x_i^j\right) \sum_{k=i-P^j}^{k=i+P^j} c_{ik}^j \Gamma\left(x_k^j\right) \\
&\quad + \lambda_3\left(v_s - x_i^j\right) \sum_{l\neq j} \Gamma\left[x_i^l(t-\tau)\right] \\
\dot{y}_i^j &= (a+\alpha)\left(x_i^j\right)^2 - y_i^j, \\
\dot{z}_i^j &= c\left(bx_i^j - z_i^j + e\right), \quad i = 1,2,\ldots,N,
\end{aligned} \tag{15}$$

where the state variable x represents the membrane potentials and, y and z correspond to the transport of ions across the membrane through the fast and slow channels respectively. The parameter c represents the ratio of the slow-fast time scale. The synaptic coupling function $\Gamma(x)$ is a nonlinear input-output function as

$$\Gamma(x) = \frac{1}{1+e^{-\lambda(x-\Theta_s)}}, \tag{16}$$

where $\lambda > 0$ determines the slope of the function and Θ_s is the firing threshold. We take the reversal potential $v_s = 2.0$ so that $v_s > x_i$ for all time t for which the synapses are excitatory and the input from other neurons to the ith neurons can enhance the activity. We choose the synaptic threshold $\Theta_s = -0.25$ and slope of the sigmoidal function $\lambda = 10$. Here $\lambda_1^j (j = 1,2)$ is the intralayer coupling strength for the jth layer. λ_3 is the interlayer synaptic coupling strength and τ is the time delay in transferring the information between the layers. The connectivity matrix $C = (c_{ik}^j)_{(n\times n)}$ is such that $c_{ik}^j = 1$ if the ith neuron is connected with kth neuron in the layer j and zero otherwise. P^j $(j = 1,2)$ is the number of neighboring oscillators in both directions connected with each oscillator in each layer. The individual oscillator exhibits square-wave bursting for a choice of parameters, $a = 2.8$, $\alpha = 1.6$, $c = 0.001$, $b = 9$, $e = 5$.

At first, we examine how interlayer coupling effects the dynamical state of the system in the absence of time delay between layers ($\tau = 0$). For the first layer we set the value of intralayer coupling strength corresponding to incoherent dynamics $\lambda_1^1 = 0.2$, while another one exhibits the chimera state $\lambda_1^1 = 1.0$. This is illustrated in Fig. 9(a), where the snapshots of $_i$ are depicted for both layers in the absence of interlayer coupling ($\lambda_3 = 0$). Unlike the KS model, this time the activation of interlayer coupling ($\lambda_3 = 0.16$) leads to the emergence of independent (i.e., asynchronous between layers) chimera states in both interconnected networks that is depicted in Fig. 9(b). By turn, the increasing of interlayer

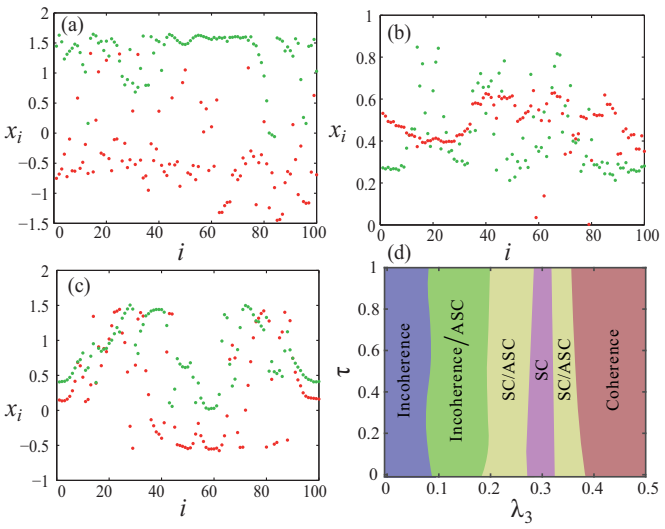

FIG. 9. Snapshots of x_i of the HR layers for (a) incoherent state in one layer (red dots) at $\lambda_1^1 = 0.2$ and chimera state in second layer (green dots) at $\lambda_1^2 = 1.0$ and $\lambda_3 = 0$, (b) asynchronous (ASC) chimera state at $\lambda_3 = 0.16$, and (c) synchronous chimera (SC) state at $\lambda_3 = 0.22$. (d) Dynamical regimes emerging in the network in a parameter space (λ_3, τ). The intralayer couplings are fixed as $\lambda_1^1 = 0.2$ and $\lambda_1^2 = 1.0$. Number of oscillators in each layer, $N = 100$.

coupling ($\lambda_3 = 0.2$) results in transition to identical regime in both layers as is clearly seen from Fig. 9(c). This illustrates the fact that in the network of Hindmarsh-Rose neurons the multiplex interaction can excite not only a synchronous interlayer chimera state, but also nonidentical chimera states in layers.

Next we consider the presence of interlayer synaptic coupling delay ($\tau \neq 0$) and check the interaction between the layers by changing the interlayer coupling strength λ_3. To get a complete overview of different spatiotemporal patterns realizing in the system, we depict the observing regime in the (τ, λ_3)-parameter space, shown in Fig. 9(d). The latter shows separate regions of incoherence, coherence, and synchronous chimera states, supplemented by areas of multistable dynamics of incoherence or asynchronous chimera and synchronous or asynchronous chimera. As mentioned above, the increasing of λ_3 leads to the transition from incoherence to independent chimera states in layers (ASC), and then to identical chimera (SC). Surprisingly, the region of synchronous chimera is divided from the coherent area by ASC or SC multistability, i.e., some increasing of λ_3 from the SC region induces a break of synchrony between layers. At the same time, any strong dependence from synaptic coupling delay (τ) cannot be observed.

VI. CONCLUSION

We explored chimera states in the framework of a multilayered network where each layer represents an ensemble of nonlocally coupled Kuramoto-Sakaguchi phase oscillators. We considered a homogeneous multilayered network where all the oscillators are identical, and a heterogeneous multilayered network where all the oscillators in each layer are identical

but there exist parameter mismatches between the layers. In the case of the two-layered network with identical parameters of layers, we observed different chimera patterns in layers for two different sets of initial phase distributions, which emerge into synchronous chimera states for large interlayer coupling interaction. Interesting is the case of networks composed from layers with different parameters, so that one layer is kept in the chimera state while the other layer is in either the coherent state or the incoherent state. Here we observed a suppression of the chimera state for moderate coupling when both layers could be almost in a coherence or an incoherent state that depends upon the status of the isolated second layer. However, synchronous chimera states or interlayer chimera states could re-emerge in the layers for larger inter-layer coupling.

We studied the interaction between two layers of the multiplexing network of phase oscillators from the viewpoint of an analytical model based on the infinite number of oscillators assumption proposed by Ott and Antonsen. We proved the possibility of interlayer chimera state excitation with increasing interlayer coupling strength. At the same time we have shown that the observed effect does not depend on the number of interacting oscillators.

We extended the results to a three-layered multiplexing network where we observed similar synchronous chimera states for large interlayer coupling. Noteworthy that the parameter space for the emergence of synchronous chimera states was broadened by the addition of a third layer. This clearly demonstrated an enhancement of the stability of chimera states by the interlayer interactions. The latter was also proven by evaluation of the more realistic model of Hindmarsh-Rose neurons, which were arranged in a two-layer multiplex network. We show that variation of interlayer coupling enables us to excite both identical (synchronous) and individual (asynchronous) chimera states in the interacting populations of model neurons. Therefore, in this system an interlayer coupling delay does not affect the dynamical features reported above. We suppose that the described phenomena could take place in real-world networks, which are usually studied, in recent times, using the framework of a multilayered model [27–32,44–47].

ACKNOWLEDGMENTS

This work has been supported by the Russian Foundation for Basic Research (Grants No. 15–52–45003 and No. 16–32–00334) and SERB-DST (Department of Science and Technology), Government of India (Project No. INT/RUS/RFBR/P-181).

[1] Y. Kuramoto and D. Battogtokh, Nonlinear Phenom. Complex Syst. **5**, 380 (2002).
[2] D. M. Abrams and S. H. Strogatz, Phys. Rev. Lett. **93**, 174102 (2004).
[3] G. C. Sethia, A. Sen, and G. L. Johnston, Phys. Rev. E **88**, 042917 (2013).
[4] I. Omelchenko, A. Zakharova, P. Hövel, J. Siebert, and E. Schöll, Chaos **25**, 083104 (2015).
[5] A. Mishra, C. Hens, M. Bose, P. K. Roy, and S. K. Dana, Phys. Rev. E **92**, 062920 (2015).
[6] Y. Kuramoto, Prog. Theor. Phys. **94**, 321 (1995); Y. Kuramoto, and H. Nakao, Phys. Rev. Lett. **76**, 4352 (1996).
[7] H. Sakaguchi and Y. Kuramoto, Prog. Theor. Phys. **76**, 576 (1986).
[8] L. Schmidt, K. Schönleber, K. Krischer, and V. García-Morales, Chaos **24**, 013102 (2014); L. Schmidt and K. Krischer, Phys. Rev. Lett. **114**, 034101 (2015).
[9] G. C. Sethia and A. Sen, Phys. Rev. Lett. **112**, 144101 (2014); A. Yeldesbay, A. Pikovsky, and M. Rosenblum, *ibid.* **112**, 144103 (2014).
[10] B. K. Bera, D. Ghosh, and M. Lakshmanan, Phys. Rev. E **93**, 012205 (2016).
[11] C. R. Laing, Phys. Rev. E **92**, 050904(R) (2015).
[12] B.-W. Li and H. Dierckx, Phys. Rev. E **93**, 020202 (2016).
[13] C. Gu, G. St-Yves, and J. Davidsen, Phys. Rev. Lett. **111**, 134101 (2013).
[14] J. Hizanidis, V. Kanas, A. Bezerianos, and T. Bountis, Int. J. Bifurcat. Chaos **24**, 1450030 (2014).
[15] B. K. Bera, D. Ghosh, and T. Banerjee, Phys. Rev. E **94**, 012215 (2016).
[16] I. Omelchenko, Y. L. Maistrenko, P. Hovel, and E. Scholl, Phys. Rev. Lett. **106**, 234102 (2011).
[17] D. P. Rosin, D. Rontani, N. D. Haynes, E. Scholl, and D. J. Gauthier, Phys. Rev. E **90**, 030902(R) (2014).
[18] M. R. Tinsley, S. Nkomo, and S. Showalter, Nat. Phys. **8**, 662 (2012).
[19] L. Larger, B. Penkovsky, and Y. L. Maistrenko, Phys. Rev. Lett. **111**, 054103 (2013); L. V. Gambuzza, A. Buscarino, S. Chessari, L. Fortuna, R. Meucci, and M. Frasca, Phys. Rev. E **90**, 032905 (2014).
[20] M. Wickramasinghe and I. Z. Kiss, PLoS ONE **8**, e80586 (2013).
[21] A. Hagerstrom, T. E. Murphy, R. Roy, P. Hövel, I. Omelchenko, and E. Schöll, Nat. Phys. **8**, 658 (2012).
[22] E. A. Martens, S. Thutupalli, A. Fourriere, and O. Hallatschek, Proc. Nat. Acad. Sci. USA **110**, 10563 (2013).
[23] J. Sieber, O. E. Omelchenko, and M. Wolfrum, Phys. Rev. Lett. **112**, 054102 (2014).
[24] R. Levy, W. D. Hutchison, A. M. Lozano, and J. O. Dostrovsky, J. Neurosci. **20**, 7766 (2000).
[25] A. E. Motter, Nat. Phys. **6**, 164 (2010).
[26] M. J. Panaggio and D. M. Abrams, Nonlinearity **28**, R67 (2015).
[27] M. Kivela, A. Arenas, M. Barthelemy, J. P. Gleeson, Y. Moreno, and M. A. Porter, J. Complex Networks **2**, 203 (2014).
[28] S. Boccaletti, G. Bianconi, R. Criado, C. I. del Genio, J. Gómez-Gardeñes, M. Romance, I. Sendiña-Nadal, Z. Wang, and M. Zanin, Phys. Rep. **544**, 1 (2014).
[29] F. Sorrentino, New J. Phys. **14**, 033035 (2012).
[30] D. Irving and F. Sorrentino, Phys. Rev. E **86**, 056102 (2012).
[31] A. Bogojeska, S. Filiposka, I. Mishkovski, and L. Kocarev, Telecommun. Forum (TELFOR), 172 (2013).
[32] R. Gutiérrez, I. Sendiña-Nadal, M. Zanin, D. Papo, and S. Boccaletti, Sci. Rep. **2**, 396 (2012).

[33] V. V. Makarov, A. A. Koronovskii, V. A. Maksimenko, A. E. Hramov, O. I. Moskalenko, J. M. Buldú, and S. Boccaletti, Chaos, Solitons Fractals **84**, 23 (2016).
[34] R. Gopal, V. K. Chandrasekar, A. Venkatesan, and M. Lakshmanan, Phys. Rev. E **89**, 052914 (2014).
[35] E. Ott and T. M. Antonsen, Chaos **18**, 037113 (2008).
[36] E. Ott and T. M. Antonsen, Chaos **19**, 023117 (2008).
[37] C. R. Laing, Physica D: Nonlin. Phenom. **238**, 1569 (2009).
[38] O. E. Omelchenko and M. Wolfrum, Phys. Rev. Lett. **109**, 164101 (2012).
[39] S. A. Marvel, R. E. Mirollo, and S. H. Strogatz, Chaos **19**, 043104 (2009).
[40] C. Xu, H. Xiang, J. Gao, and Zh. Zheng, Sci. Rep. **6**, 31133 (2016).
[41] G. Bordyugov, A. Pikovsky, and M. Rosenblum, Phys. Rev. E **82**, 035205 (2010).
[42] H. Hong and S. H. Strogatz, Phys. Rev. E **84**, 046202 (2011).
[43] B. K. Bera and D. Ghosh, Phys. Rev. E **93**, 052223 (2016).
[44] F. Battiston, V. Nicosia, and V. Latora, Phys. Rev. E **89**, 032804 (2014).
[45] M. De Domenico, A. Solé-Ribalta, E. Cozzo, M. Kivelä, Y. Moreno, M. A. Porter, S. Gómez, and A. Arenas, Phys. Rev. X **3**, 041022 (2013).
[46] L. Solá, M. Romance, R. Criado, J. Flores, A. G. del Amo, and S. Boccaletti, Chaos **23**, 033131 (2013).
[47] B. Min, S. D. Yi, K. M. Lee, and K. I. Goh, Phys. Rev. E **89**, 042811 (2014).